Phase-matching spectral phase measurement and domain period reconstruction of aperiodic quasi-phase matched gratings by nonlinear spectral interferometry

Chia-Lun Tsai,[1] Ming-Chi Chen,[1] Jui-Yu Lai,[1,2] Dong-Yi Wu,[2] and Shang-Da Yang[1,*]

[1]*Institute of Photonics Technologies, National Tsing Hua University, Hsinchu 30013, Taiwan*
[2]*HC Photonics Corp., R&D Division, 4F, No. 2, Technology Rd. V, Hsinchu Science Park, Hsinchu 30078, Taiwan*
[*]*shangda@ee.nthu.edu.tw*

Abstract: We experimentally measured the phase-matching spectral phases of aperiodic quasi-phase matched gratings for the first time (to the best of our knowledge) by nonlinear spectral interferometry. The retrieved information is useful in determining the temporal shape of the nonlinearly converted ultrafast signal and reconstructing the slowly-varying domain period distribution. The method is nondestructive, fast, sensitive, accurate, and applicable to different nonlinear materials. Compared to taking microscopic images of the etched crystal surface, our method can directly measure the domain period distribution in the crystal interior and is free of the artificial random duty period error due to image concatenation.

OCIS codes: (120.3180) Interferometry; (120.5050) Phase measurement; (230.4320) Nonlinear optical devices.

References and links

1. M. M. Fejer, G. A. Magel, D. H. Jundt, and R. L. Byer, "Quasi-phase-matched second harmonic generation: tuning and tolerances," IEEE J. Quantum Electron. **28**(11), 2631–2654 (1992).
2. M. Asobe, O. Tadanaga, T. Umeki, T. Yanagawa, Y. Nishida, K. Magari, and H. Suzuki, "Unequally spaced multiple mid-infrared wavelength generation using an engineered quasi-phase-matching device," Opt. Lett. **32**(23), 3388–3390 (2007).
3. J.-Y. Lai, C.-W. Hsu, N. Hsu, Y.-H. Chen, and S.-D. Yang, "Hyperfine aperiodic optical superlattice optimized by iterative domino algorithm for phase-matching engineering," Opt. Lett. **37**(7), 1184–1186 (2012).
4. J.-Y. Lai, C.-W. Hsu, D.-Y. Wu, S.-B. Hung, M.-H. Chou, and S.-D. Yang, "Healing block-assisted quasi-phase matching," Opt. Lett. **38**(7), 1176–1178 (2013).
5. C. Heese, C. R. Phillips, L. Gallmann, M. M. Fejer, and U. Keller, "Ultrabroadband, highly flexible amplifier for ultrashort midinfrared laser pulses based on a periodically poled Mg:$LiNbO_3$," Opt. Lett. **35**(14), 2340–2342 (2010).
6. U. Kornaszewski, M. Kohler, U. K. Sapaev, and D. T. Reid, "Designer femtosecond pulse shaping using grating-engineered quasi-phase-matching in lithium niobate," Opt. Lett. **33**(4), 378–380 (2008).
7. G. H. C. New, "Theory of pulse compression using aperiodic quasi-phase-matched gratings," J. Opt. Soc. Am. B **24**(5), 1144–1149 (2007).
8. J. S. Pelc, C. R. Phillips, D. Chang, C. Langrock, and M. M. Fejer, "Efficiency pedestal in quasi-phase-matching devices with random duty-cycle errors," Opt. Lett. **36**(6), 864–866 (2011).
9. W. H. Peeters and M. P. van Exter, "Optical characterization of periodically-poled $KTiOPO_4$," Opt. Express **16**(10), 7344–7360 (2008).
10. C. Langrock, private communication (2012).
11. R. Trebino, in *Frequency-Resolved Optical Gating: The Measurement of Ultrashort Laser Pulses* (Kluwer Academic Publishers, 2000).
12. S. K. Johansen and P. Baldi, "Characterization of quasi-phase-matching gratings in quadratic media through double-pass second-harmonic power measurements," J. Opt. Soc. Am. B **21**(6), 1137–1145 (2004).
13. L. Lepetit, G. Chériaux, and M. Joffre, "Linear techniques of phase measurement by femtosecond spectral interferometry for applications in spectroscopy," J. Opt. Soc. Am. B **12**(12), 2467–2474 (1995).
14. O. Gayer, Z. Sacks, E. Galun, and A. Arie, "Temperature and wavelength dependent refractive index equations for MgO-doped congruent and stoichiometric $LiNbO_3$," Appl. Phys. B **91**(2), 343–348 (2008).

#187047 - $15.00 USD Received 14 Mar 2013; revised 1 May 2013; accepted 2 May 2013; published 7 May 2013

1. Introduction

Designs and applications of aperiodic quasi-phase matched (QPM) gratings have been intensively explored during the past two decades [1–7]. For example, an arbitrary nonlinear conversion efficiency spectrum can be achieved by optimizing the domain orientation distribution $g(x)$ (defined in [1]) and has been applied to the detection of multiple hydrocarbon gases [2,3]. Chirped QPM gratings with broadened and tailored complex phase-matching (PM) responses $H(\Omega)$ [defined in Eq. (1)] were used in parametric amplification of few-cycle mid-infrared pulse [5] and second-harmonic pulse shaping [6,7], respectively. Applications of aperiodic QPM can be facilitated by the ability to measure $H(\Omega)$ experimentally for two reasons. First, the temporal shaping of the nonlinear signal depends on $H(\Omega)$, which could deviate from the design due to the increased poling error in the presence of different domain sizes [6]. Second, the domain period function $\Lambda(x)$, or even the domain orientation distribution $g(x)$, can be reconstructed if $H(\Omega)$ and the dispersion relation are known. In contrast to measuring the statistical information (e.g. random duty cycle error) of periodic QPM gratings by analyzing the PM efficiency pedestal [8] or Maker fringes [9], this approach would allow the convenient determination of the slowly-varying $\Lambda(x)$ or deformations of aperiodic QPM structures arising from lithographic patterning error in the presence of uneven substrates [10]. There exist some methods able to measure $H(\Omega)$ or $g(x)$ experimentally. (1) Under the assumptions of plane waves, non-depleted pump, and negligible group velocity dispersion, the second-harmonic spectral envelope is given by a transfer function relation [1]:

$$A_{2\omega}(\Omega) = P_{NL}(\Omega) \times H(\Omega), \tag{1}$$

where $P_{NL}(\Omega) = A_{\omega} \otimes A_{\omega}$ is the nonlinear polarization spectrum of the fundamental spectral envelope $A_{\omega}(\omega)$. As a result, $H(\Omega)$ can be determined by simultaneously measuring the fundamental and second-harmonic fields $A_{\omega}(\omega)$ and $A_{2\omega}(\Omega)$. However, measuring $A_{2\omega}(\Omega)$ typically requires another nonlinear conversion process [e.g. second-harmonic generation (SHG) or parametric amplification] [11], which is subject to worse sensitivity, accumulated error, and higher risk that the converted wavelengths become absorptive in the nonlinear medium. (2) A double-pass SHG scheme was proposed to measure $g(x)$ of arbitrary QPM gratings nondestructively [12], but has not been experimentally verified. (3) Taking local microscopic images of the etched surface of a QPM grating, and concatenating them to obtain the global $g(x)$. In addition to the enormous time and effort required in sample preparation, image taking, and signal processing, this method suffers from errors due to image concatenation (artificial random duty period error) and non-uniformly poled cross-section that could be substantial for short-period or thick QPM gratings (Fig. 1).

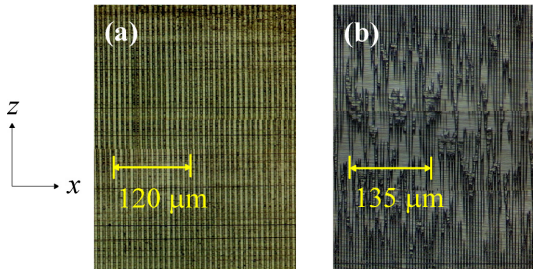

Fig. 1. Microscopic side views of two z-cut periodically poled MgO-doped lithium niobate (PPMgLN) samples with (a) uniformly, and (b) non-uniformly poled cross-sections, respectively. Dark regions represent the inverted domains.

In this paper, we propose a scheme based on nonlinear spectral interferometry (NLSI) to measure the phase of $H(\Omega)$ and reconstruct the domain period function $\Lambda(x)$. The functions of $H(\Omega)$ and $\Lambda(x)$ of aperiodically poled MgO-doped lithium niobate (A-PPMgLN) samples

#187047 - $15.00 USD Received 14 Mar 2013; revised 1 May 2013; accepted 2 May 2013; published 7 May 2013

were experimentally measured by NLSI and microscopic images (of the HF-etched surfaces), respectively. They were analyzed and compared with those defined by the lithographic masks. NLSI is nondestructive, fast, sensitive, accurate, and applicable to different nonlinear materials. It is free of the artificial random duty period error, and can directly measure the domain period distribution in the crystal interior (where optical beam normally accesses).

2. Theory

Spectral interferometry is a linear technique used in measuring the spectral phase difference between two optical waves of the same carrier frequency [13]. In NLSI, the signal and reference waves come from SHG of a common fundamental field of carrier frequency ω_0 and spectral envelope $A_\omega(\omega)$ passing through a test QPM grating and a reference thin nonlinear crystal with complex PM responses $H(\Omega) = |H(\Omega)| \times \exp[j\psi(\Omega)]$ and $H_r(\Omega) = |H_r(\Omega)| \times \exp[j\psi_r(\Omega)]$ (Ω denotes the angular frequency detuning from $2\omega_0$), respectively. According to Eq. (1), the spectral envelopes of the (second-harmonic) signal and reference waves are $A_s(\Omega) = P_{NL}(\Omega) \times H(\Omega)$ and $A_r(\Omega) = P_{NL}(\Omega) \times H_r(\Omega)$, respectively. If the two waves are temporally separated by a delay τ, the resulting power spectrum (interferogram) becomes

$$S(\Omega) = |A_s(\Omega)|^2 + |A_r(\Omega)|^2 + 2|A_s(\Omega) \times A_r(\Omega)| \times \cos[\tau\Omega - \angle A_s(\Omega) + \angle A_r(\Omega) + 2\omega_0\tau], \quad (2)$$

where the symbol $\angle Z$ means the phase of Z. Equation (2) shows that the spectral phase difference function $\Delta\psi(\Omega) = \angle A_s(\Omega) - \angle A_r(\Omega)$ can be retrieved by Fourier analysis of $S(\Omega)$ [13]. Since $\angle A_s(\Omega) = \angle P_{NL}(\Omega) + \psi(\Omega)$, $\angle A_r(\Omega) = \angle P_{NL}(\Omega) + \psi_r(\Omega)$, the phase difference $\Delta\psi(\Omega) = \psi(\Omega) - \psi_r(\Omega)$ is independent of the phase of $P_{NL}(\Omega)$. This means that the fundamental spectral phase $\angle A_\omega(\omega)$ is unimportant, and a broadband light source (regardless of its chirp) is sufficient for NLSI. Besides, $\Delta\psi(\Omega)$ will be equal to the desired PM spectral phase $\psi(\Omega)$ if the reference crystal is sufficiently thin such that $\psi_r(\Omega)$ is nearly constant within the spectral range of interest. By measuring SHG yield as a function of input wavelength, one can independently determine the PM spectral intensity $|H(\Omega)|^2$ and thus the complex $H(\Omega)$.

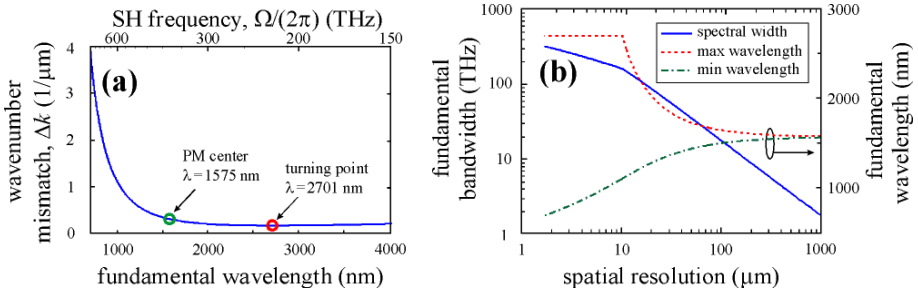

Fig. 2. Dependence of spatial resolution on source bandwidth. (a) SHG wavenumber mismatch Δk of PPMgLN versus fundamental wavelength λ. (b) The fundamental frequency bandwidth (solid) and boundary wavelengths (dotted, dashed-dotted) versus the corresponding spatial resolution of the reconstructed $g(x)$ of a PPMgLN with 1575-nm central PM wavelength. The maximum wavelength (dashed) is ceiled due to the increasing Δk for λ>2701 nm shown in (a).

Under the same assumptions that validate Eq. (1), $H(\Omega)$ of a QPM grating of length L and refractive index spectrum $n(\omega)$ is related to the domain orientation function $g(x)$ via

$$H(\Omega) \propto \int_0^L g(x) e^{i\Delta k \cdot x} dx, \quad \Delta k = (\Omega/c) \times [n(\Omega) - n(\Omega/2)]. \quad (3)$$

As a result, $g(x)$ can be reconstructed by a three-step procedure. (1) Converting the variable Ω to Δk according to the dispersion relation $n(\omega)$ [Fig. 2(a)]. (2) Performing Fourier transform (FT) for $H(\Delta k)$. (3) Determining the polarity of $g(x)$ by thresholding. Note that the missing linear phase of $H(\Omega)$ (if delay τ is not calibrated) coupled with the nonlinear relation between

#187047 - $15.00 USD Received 14 Mar 2013; revised 1 May 2013; accepted 2 May 2013; published 7 May 2013

Δk and Ω only incur nominal error for $g(x)$ unless the bandwidth is extremely broad. The FT relation between $g(x)$ and $H(\Omega)$ implies that the spatial resolution of the reconstructed $g(x)$ scales with the spectral window of the measured $H(\Omega)$ or the fundamental light source. Figure 2(b) shows that a larger fundamental bandwidth is required to improve the spatial resolution of the reconstructed $g(x)$, where an A-PPMgLN [14] with 1575-nm central PM wavelength and no nonlinear process other than SHG are assumed in the simulation. The spatial resolution is limited by ~1.7 μm (requiring a light source spanning 700-2701 nm) due to the lithium niobate absorption for wavelengths shorter than 350 nm.

3. Experimental results

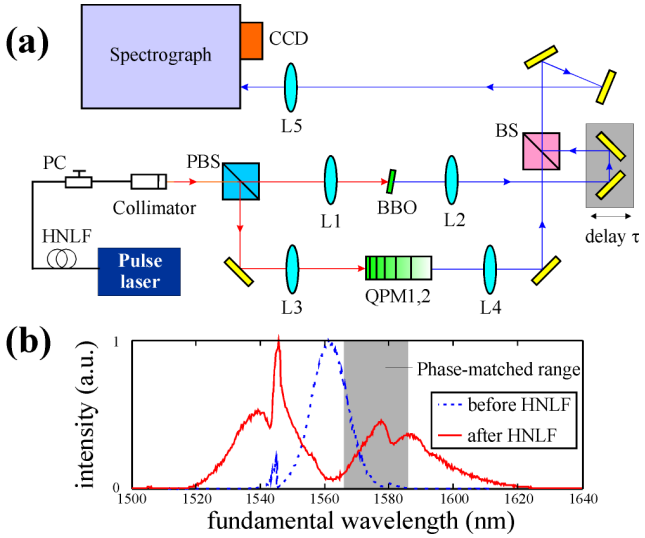

Fig. 3. (a) Experimental setup. HNLF: Highly nonlinear fiber. PC: Polarization controller. PBS: Polarization beamsplitter. L#: Lens. BS: Beamsplitter. (b) Power spectra before (dotted) and after (solid) the HNLF, respectively. The shaded area indicates the phase-matched spectral range of QPM1 and QPM2.

Figure 3(a) shows the experimental setup of NLSI. A mode-locked fiber laser produces 50 MHz, 300 fs pulses at 1560 nm. The −10 dB bandwidth is broadened from 24 nm to 79 nm [dotted and solid curves, Fig. 3(b)] by passing the pulse through a 15-m-long highly nonlinear fiber. The p-wave and s-wave components are separated by a polarization beamsplitter, focused into a 1-mm-long Type-I BBO reference crystal and a 49.5-mm-long A-PPMgLN with different types of QPM gratings (HC Photonics) to generate the second-harmonic reference and signal pulses, respectively. The mask-defined domain period distributions $\Lambda(x)$ of QPM1 and QPM2 are linear and quadratic functions monotonically decreasing from 20.4 μm to 19.9 μm, corresponding to phase-matched fundamental wavelengths of 1566-1586 nm [shaded, Fig. 3(b)]. A polarization controller is used to maximize the fringe contrast of the interferogram $S(\Omega)$ by controlling the power ratio of the two arms. The two s-polarized second-harmonic pulses are delayed with each other, recombined by a beamsplitter, focused into a spectrograph, and recorded by an un-cooled CCD array to get the interferogram $S(\Omega)$. In our experiment, 12-μW average fundamental power and 100-ms CCD integration time would be sufficient for accurate measurements. The broad input spectral width and the short BBO crystal (phase-matched wavelengths are beyond 1520-1630 nm) ensure that the fringes of $S(\Omega)$ exist for the entire spectral range of $H(\Omega)$ of each QPM grating [a prerequisite of measuring $\psi(\Omega)$].

#187047 - $15.00 USD Received 14 Mar 2013; revised 1 May 2013; accepted 2 May 2013; published 7 May 2013

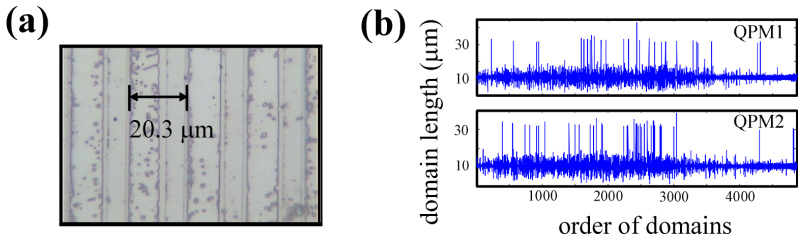

Fig. 4. (a) A microscopic image of QPM1 with more than 8 domains. (b) The global domain length distributions of QPM1, QPM2 obtained by concatenating ~620 microscopic images.

Figure 4(a) shows a sample microscopic image of the QPM1 surface, from which we can measure the local domain lengths. The global domain length distributions [Fig. 4(b)] of QPM1, QPM2 were obtained by combining the results of ~620 images taken from each of the two QPM gratings. In addition to the majority lengths around 10 μm, there are 30 and 40 "long domains" (~30 μm) out of the total 4925 and 4948 "mask-defined" domains in QPM1 and QPM2, respectively. This is attributed to the domain inversion failure such that three neighboring mask-defined domains merge into a 3-time-longer domain.

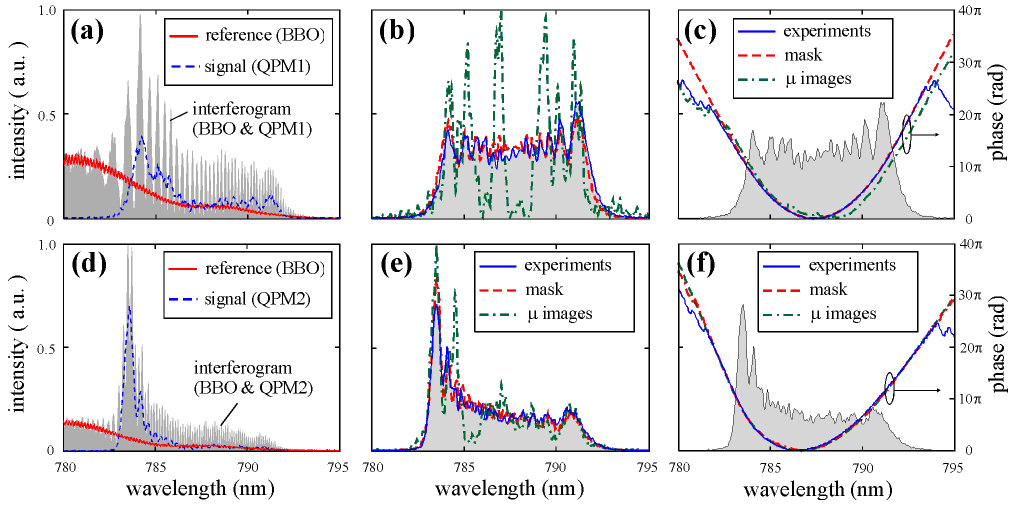

Fig. 5. Experiment results of (a-c) QPM1 and (d-f) QPM2. (a,c) Second-harmonic power spectra of the reference (solid), signal (dashed), and their interferogram (shaded). (b,c,e,f) PM spectral intensities and phases obtained by experiments (solid and shaded), lithographic mask function (dashed), and microscopic images (dashed-dotted), respectively.

Figures 5(a) and 5(d) illustrate the second-harmonic power spectra of the reference pulse (solid), the signal pulse (dashed), and their interferogram $S(\Omega)$ (shaded) due to QPM1 and QPM2, respectively. The fringe density of either $S(\Omega)$ increases with wavelength, consistent with a down-chirped second-harmonic signal pulse caused by a QPM grating with monotonically decreasing domain period function $\Lambda(x)$. Figures 5(b) and 5(e) show the PM power spectra of QPM1 and QPM2 obtained by three methods: (1) wavelength-scanning SHG experiment (solid and shaded), (2) FT of the mask-defined $g(x)$ (dashed), (3) FT of the microscopically imaged $g(x)$ (dashed dotted), respectively. It is evident that the artificial random duty period error due to concatenating a large number of microscopic images may result in seriously distorted PM power spectra. The curves in Figs. 5(c) and 5(f) represent the PM spectral phases of QPM1 and QPM2 obtained by NLSI experiment ψ_{exp} (solid), mask function ψ_m (dashed), and microscopic images ψ_μ (dashed-dotted), respectively. The accuracy of PM spectral phase measurement can be quantitatively estimated by the intensity-weighted root-mean-square (rms) phase error

#187047 - $15.00 USD Received 14 Mar 2013; revised 1 May 2013; accepted 2 May 2013; published 7 May 2013

$$\varepsilon_{\mathrm{rms}} \equiv \sqrt{\sum_{i=1}^{N}\left[\psi_{\exp}(\lambda_i)-\psi(\lambda_i)\right]^2 \times \left|H(\lambda_i)\right|^2 \Big/ \sum_{i=1}^{N}\left|H(\lambda_i)\right|^2}, \qquad (4)$$

where $|H(\lambda_i)|^2$ is the phase-matching power spectrum, and λ_i (i = 1-N) indicates the ith sampling wavelength. The rms phase errors between $\psi_{\exp}$ and ψ_{m} are 0.36π (QPM1) and 0.31π (QPM2), better than 1.46π (QPM1) and 0.32π (QPM2) between ψ_{μ} and ψ_{m}. Since these $\varepsilon_{\mathrm{rms}}$ values are much smaller than the overall phase range (~40π), our method is reasonably accurate.

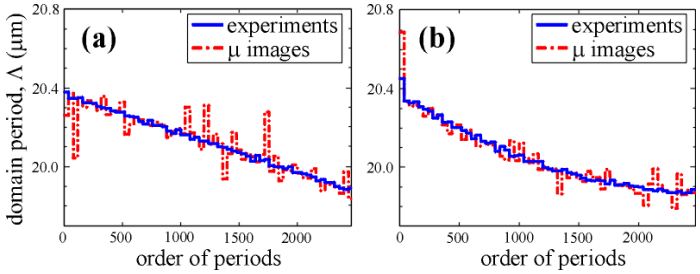

Fig. 6. Domain period distributions measured by experiments (solid) and microscopic images (dashed-dotted) for (a) QPM1, and (b) QPM2, respectively.

Figure 6 shows the domain period functions $\Lambda_{\exp}(x)$ and $\Lambda_{\mu}(x)$ measured by (NLSI and wavelength-scanning SHG) experiments and microscopic images, respectively. Simulation [Fig. 2(b)] shows that the spectral window (783-792 nm) of the interferogram enables a spatial resolution of 810 μm. As a result, we reduced the spatial resolution of the raw domain period functions to ~800 μm by piecewise average. This resolution can reveal the slowly-varying domain periods due to mask design or undesired lithographic patterning error [10], but is insufficient to identify the ~30-μm "long domains". As shown in Figs. 6(a) and 6(b), $\Lambda_{\exp}(x)$ and $\Lambda_{\mu}(x)$ of QPM1 and QPM2 indeed resolve the linear and quadratic trends of $\Lambda_{\mathrm{m}}(x)$ defined by the lithographic masks. The bumpy $\Lambda_{\mu}(x)$ curves are primarily due to the uncertainty (~0.2 μm) in positioning the domain boundaries of microscopic images. The mean and standard deviation of the period difference $\Delta\Lambda(x) = |\Lambda_{\exp}(x)-\Lambda_{\mu}(x)|$ are 41 nm and 58 nm for QPM1, or 31 nm and 39 nm for QPM2, respectively.

4. Conclusions

We experimentally retrieved the phase-matching spectral phases of aperiodic QPM gratings for the first time (to the best of our knowledge) by using nonlinear spectral interferometry. The complex phase-matching responses and domain period distributions of aperiodic QPM gratings measured by NLSI and microscopic images are in good agreement with those defined by the lithographic masks. Our method is nondestructive, fast (only acquiring one power spectrum and using non-iterative phase retrieval), sensitive (using only one nonlinear conversion process), accurate, applicable to different nonlinear materials, and independent of the chirp of the fundamental light source. Compared to taking microscopic images of the etched crystal surface, our method can directly measure the domain period distribution in the crystal interior (normally accessed by the optical beams) and is free of the artificial random duty period error due to image concatenation.

Acknowledgment

This material is based on research supported by the National Science Council of Taiwan under grants NSC-99-2120-M-007-010, and NSC-100-2221-E-007-093-MY3 and by the National Tsing Hua University under grant 101N2081E1.